LARGE-AMPLITUDE FINITE ELEMENT FLUTTER ANALYSIS OF COMPOSITE PANELS IN HYPERSONIC FLOW

Carl E. Gray, Jr.*
NASA Langley Research Center, Hampton, Virginia 23665

Chuh Mei[†]
Old Dominion University, Norfolk, Virginia 23529

ABSTRACT

A finite-element approach is presented for determining the nonlinear flutter characteristics of three-dimensional thin laminated composite panels using the full third-order piston, transverse loading, aerodynamic theory. The unsteady, hypersonic, aerodynamic theory and the von Karman large deflection plate theory are used to formulate the aeroelasticity problem. Nonlinear flutter analyses are performed to assess the influence of the higher-order aerodynamic theory on the structure's limit-cycle amplitude and the dynamic pressure of the flow velocity. A solution procedure is presented to solve the nonlinear panel flutter finite element equations. Nonlinear flutter analyses are performed for different boundary support-conditions and for various system parameters: aspect ratio a/b; material orthotropic ratio, lamination angle θ, and number of layers; Mach number, M; flow mass-density-to-panel-mass-density ratio, μ/M; dynamic pressure, λ; and maximum-deflection-to-thickness ratio, c/h. The large-amplitude panel flutter results using the full third-order piston aerodynamic theory are presented to assess the influence of the nonlinear aerodynamic theory.

NOMENCLATURE

a, b	panel length and width
$[a]$	element aerodynamic matrix
$[\mathcal{A}]$	panel aerodynamic matrix
$[A], [B], [D]$	laminate stiffness matrices
c	maximum panel deflection
$[C_\theta]$	matrix relating element displacements to membrane-bending strains
D_c	composite panel rigidity parameter
$\{e\}$	membrane strains
E, E_{11}, E_{22}	isotropic and lamina elastic modulus
$[g]$	element aerodynamic damping matrix
$[G]$	panel aerodynamic damping matrix
G, G_{12}	isotropic and lamina shear modulus
h	panel thickness
$[k]$	element stiffness matrix
M	Mach number
$[m]$	element mass matrix
$[M]$	panel mass matrix
$\{\mathcal{N}_A\}$	linearized midsurface force associated with $[A]$
$\{\mathcal{N}_B\}$	linearized midsurface force associated with $[B]$
p, p_∞	aerodynamic pressure
$[Pu], [Pw]$	matrix relating element displacements to membrane strains and curvatures
q	dynamic pressure
$[\bar{Q}]$	transformed reduced lamina stiffness matrices
u, v, w	in-plane and transverse panel displacements
V	flow velocity
$\{\Delta u\}, \{\Delta v\}, \{\Delta w\}$	plate element displacements
$\{U\}, \{V\}, \{W\}$	global finite element displacements
x, y, z	Cartesian coordinates

Greek symbols

α	real part of eigenvalue
β	eigenvalue phase angle
γ	ratio of specific heats, $\gamma = 1.4$
δ	variational operator
$\{\epsilon\}$	strain vector
θ	lamination angle
$[\Theta]$	linearized displacement matrix
$\{\kappa\}$	laminate bending curvatures
λ	non-dimensional dynamic pressure
μ	$\rho_a a / \rho h$
ν	Poisson's ratio, $\nu = .3$ for isotropic
ρ, ρ_a	panel mass density and air mass density
$\{\sigma\}$	stress vector
ϕ	interpolation functions

*Aerospace Engineer, Facilities Engineering Division. Senior Member AIAA.

[†]Professor, Department of Mechanical Engineering and Mechanics. Associate Fellow AIAA.

$\{\Phi\}$	complex eigenvector
ω	imaginary part of eigenvalue
Ω	complex eigenvalue, $\alpha + i\omega$

INTRODUCTION

Aircraft flight into the supersonic regime, during the 1950's, stressed the conflicting conditions of fabricating a structure strong enough to withstand large aerodynamic forces during supersonic flight, yet light enough to be economically efficient to allow for an increase in the flight vehicle's payload capability. Because of the resurgent interest in flight vehicles such as the High-Speed Civil Transport (HSCT), the National Aero-Space Plane (NASP), and the Advanced Tactical Fighter (ATF) that will operate not only at high-supersonic Mach numbers but well into the hypersonic regime, the additional requirement for energy-efficient, high-strength and minimum-weight vehicles has become apparent. These requirements have generated an interest in the advanced composite materials to meet the high-strength minimum-weight requirements. In addition to the structural material concerns, the issue of the range of applicability of the widely used first-order piston aerodynamic theory into the hypersonic regime has been questioned. These questions have been generated in response to neglecting the higher-order terms in the derivation of the first-order theory. It has been hypothesized that the higher-order terms in the piston aerodynamic theory, at the large Mach numbers of interest, may be significant. Coupling these concerns with the realistic need for analytical tools to evaluate complex structures, the finite element method presents itself as the most appropriate means that can conveniently and efficiently incorporate all of the known complexities of the physical problem.

Theoretical considerations of panel flutter using linear theory, as well as an early survey on the subject up to 1966, was given by Dungundji [1][1]. A thorough summary on both linear and nonlinear panel flutter through 1970 was given by Dowell [2]. Most recently, 1987, Reed, Hanson, and Alford [3], conducted a survey in the area of hypersonic panel flutter in support of the NASP program. As disclosed by all of these survey papers, a great quantity of literature exists on linear panel flutter using different aerodynamic theories, for example references [1,4,5] and many others. The aerodynamic theory employed for the most part for panel flutter at high supersonic Mach numbers ($M > 1.7$ [5]) is the quasi-steady first-order piston aerodynamic theory [6]. Because of the recent renewed interest [3] in flight vehicles that will operate not only at high-supersonic Mach numbers but well into the hypersonic regime, there is an interest in approaches that can employ unsteady nonlinear aerodynamic theories. The piston aerodynamic theories, although several decades old, have generally been employed to approximate the aerodynamic loads on the panel from local pressures generated by the body's motion as related to the local normal component of the fluid velocity. This theory, thus, defines a point-function relationship between the normal component of the fluid velocity and the local panel pressure. For supersonic Mach numbers, these theories reasonably estimate the aerodynamic pressures and are the most widely used in the literature. An outstanding presentation of the fundamental theories and the physical understanding of panel flutter can be found in the book on the subject by Dowell [7].

In actuality, it is well known [8] that the panel not only bends but also stretches due to large-amplitude vibrations. Such membrane tensile forces in the panel, due to the induced stretching, provides a limited stabilizing effect of the "hard spring" type that restrains the panel motion to be of bounded amplitude for limit-cycle oscillations that increases with amplitude as the dynamic pressure, λ_ℓ, increases. The external skin of a flight vehicle can,

thus, withstand velocities beyond the linear critical value. McIntosh [9] has investigated the effects of hypersonic nonlinear aerodynamic loadings on panel flutter, and his findings indicate that the higher-order aerodynamic theory may, for some system parameters, produce a "soft spring" effect that will predict lower limit-cycle flutter velocities than those predicted by the first-order piston theory even including the effect of membrane tensile forces in the panel. In reference [2], Dowell identifies four panel flutter theories, types 1–4 shown in Table 1, and with the theory in reference [9] these theories increase to five.

The first partial nonlinear behavior of a fluttering panel was studied by several investigators: Bolotin [10], Fung [11], Houbolt [12], and Eisely [13]. They were primarily concerned with determining stability boundaries of two-dimensional plates. Using a two-mode Galerkin approach, the three-dimensional plate buckling effects on flutter boundaries using the von Karman deflection theory and Ackert's aerodynamic theory (also known as a static strip theory [5,14]) was studied by Fralich [15].

For the full structural nonlinear limit-cycle approach, a variety of analysis methods have been employed to assess the panel flutter problem. The direct numerical integration approach in conjunction with Galerkin's method was first used by Dowell [16–18] to study the nonlinear oscillations of simply supported, in-plane elastically restrained, fluttering plates. Dowell determined that the direct numerical integration (classical) approaches required as a minimum six linear normal modes to achieve a converged solution for displacements and possibly more if stresses are required [9,18]. For the clamped plates, Ventres [19] also used the direct numerical integration method by employing both the quasi-steady aerodynamic theory and the generalized aerodynamic theory, type 3 analysis. Both Dowell and Ventres used the Galerkin's method to reduce the governing partial differential equations in time and space to a set of coupled ordinary differential equations in time which were numerically integrated for arbitrary initial conditions. The integration was continued until a limit-cycle oscillation of constant amplitude, that was independent of the initial conditions, was encountered. But because of the highly nonlinear nature of the aerodynamic theory, there exists just a few references that have investigated the limit-cycle oscillations of panels for hypersonic flow. McIntosh [9], using a nonlinear, partial third-order piston aerodynamic theory, also integrated the nonlinear equations of motion for given initial conditions and observed the resultant panel motion versus time until a limit-cycle of constant amplitude was reached.

A number of other classical analytical methods exist for the investigation of limit-cycle oscillations of panels in supersonic flow. In general, for the supersonic case, Galerkin's method is used in the spatial domain, and the panel deflection is then expressed in terms of two to six linear normal modes. Various techniques in the temporal domain such as harmonic balance [10, 20–23] have been used successfully to study the subject of panel flutter. This method requires less computational time than the method of direct integration and is mathematically comprehensible and systematic, but extremely tedious to implement. Another popular method to study panel flutter is the perturbation method. Correlation between perturbation techniques and the harmonic balance method has been shown to be quite good [21,24,25].

Most of the early research in panel flutter using classical analytical methods [26–30] has been limited to orthotropic panels (or plates). Recently, a considerable focus has turned to the application of anisotropic materials. However, most of this work has been limited to the area of linear structural theory using classical laminated plate theory. Librescu [31], retaining only the linear aerodynamic damping terms, derived the governing equations for an arbitrary number of modes using Galerkin's method and the Lyapunov stability criterion. He investigated the aeroelastic stability of orthotropic panels in the vicinity of the critical dynamic pressure. The geometric nonlinear flutter of orthotropic panels was recently studied by Eslami [32,33] using harmonic balance. All of the analytical investigations have

---

[1]Numbers in brackets indicate reference.

1282

been limited to two-dimensional or three-dimensional rectangular plates with all four edges simply supported or clamped.

Extension of the finite element method to study the linear panel flutter problem was due to Olson [34,35]. Because of its versatile applicability, effects of aerodynamic damping, complex panel configurations, flow angularities, in-plane prestress, and laminated anisotropic panel properties can be easily and conveniently included in the finite element formulation. A review of the linear panel flutter using finite element methods was given by Yang and Sung [36].

Application of the finite element method to study the supersonic limit-cycle oscillations of two-dimensional panels was given by Mei and Rogers [37] and Mei [38]. Rao and Rao [39] also investigated the large-amplitude supersonic flutter of two-dimensional panels with ends elastically restrained against rotation. Mei and Weidman [40], Han and Yang [41], and Mei and Wang [42] further extended the finite element method to treat supersonic limit-cycle oscillations of three-dimensional rectangular and triangular isotropic plates, respectively.

Sarma and Varadan [43] studied the nonlinear behavior of two-dimensional isotropic panels using the linear aerodynamic theory. They presented two solution methods using a seventh-order displacement based finite element; the first method uses the nonlinear free vibration mode shape as an approximation to the nonlinear panel flutter problem, and the second method uses the linear panel flutter mode shape as an initial estimate for an iterative solution process similar to those given in Refs. [37–42, and 45–47]. Because of the renewed interest in panel flutter at the high-supersonic/hypersonic speeds, Gray, et al. [44] extend the finite element method to investigate the hypersonic limit-cycle oscillations of two-dimensional panels. A treatment of the aeroelastic concepts and principles is covered at the fundamental level in Refs. [48–50].

FINITE ELEMENT FORMULATION

Consider a three-dimensional laminated panel of length a, width b, thickness h, and mass density ρ with a fluid flow above the panel at Mach number M. It is assumed that fluid flow above the panel is in the positive x coordinate direction and that the effects of the cavity on the back side of the panel can be neglected. The sign convention to be followed is that positive flow is in the direction of increasing x and a positive deflection is into the cavity. Since this study addresses thin panels ($a/h > 50$), the effect of transverse shear deformations, normally associated with thick plates (laminates) is neglected (see Jones [51] for example). This assumption is justified due to the minimum weight constraint that generally drives the panel's design parameters such that a/h is greater than 100.

Hamilton's Principle for a Continuum

The most general form of Hamilton's principle for a nonconservative elastic continuous medium is

$$
\int_{t_1}^{t_2} \left[\int_V (\rho \vec{u}_{,tt} \cdot \delta \vec{u}) \, dV - \left(\int_V \left(\vec{f} \cdot \delta \vec{u} \right) dV \right. \right.
$$
$$
\left. \left. + \int_S (\vec{p} \cdot \delta \vec{u}) \, dS - \int_V (\sigma : \delta \epsilon) dV \right) \right] dt = 0 \qquad (1)
$$

where S and V are the surface area and volume of the element, respectively. The terms under the time integral represent the work done on the body at any time t by the resultant force in moving through the virtual displacement $\delta \vec{u}$; $\vec{f}$ is the body force, and is neglected in this formulation; $\vec{p}$ is the specified surface stress vector; and $(\sigma : \delta \epsilon)$ is a stress-virtual strain-tensor product.

Constitutive and Strain-Displacement Relationships

Since for the three-dimensional panel, there are two primary material directions, the formulation will be for the most general anisotropic laminated material of which an isotropic material is a special case. For an orthotropic lamina [51], the stress-strain relationship in x-y coordinates is

$$
\{\sigma\} = \left\{ \begin{array}{c} \sigma_x \\ \sigma_y \\ \tau_{xy} \end{array} \right\} = [\bar{Q}] \left\{ \begin{array}{c} \epsilon_x \\ \epsilon_y \\ \gamma_{xy} \end{array} \right\} = [\bar{Q}]\{\epsilon\} \qquad (2)
$$

The bar over the $\bar{Q}_{ij}$ denotes the transformed reduced stiffnesses relative to the x-y-z coordinate.

The form of the strain-displacement relationships for an arbitrary point through the thickness, h, is as follows:

$$
\epsilon_x = u_{,x} + \frac{1}{2} w_{,x}^2 - z w_{,xx}
$$
$$
\epsilon_y = v_{,y} + \frac{1}{2} w_{,y}^2 - z w_{,yy} \qquad (3)
$$
$$
\gamma_{xy} = u_{,y} + v_{,x} + w_{,x} \, w_{,y} - 2 z w_{,xy}
$$

where u and v are the in-plane (midsurface) displacements measured along the x and y coordinate axes, respectively, and w is the transverse displacement measured along the z-axis normal to the plane of the panel. The nonlinear terms in Eq. (3) are commonly referred to as the von Karman nonlinear (finite) strains.

Aerodynamic Pressure Function

The virtual work integral involving the surface stress vector is evaluated using the unsteady full third-order piston theory aerodynamics [6] to develop the aerodynamic loads on the upper surface of the panel. The aerodynamic pressure loading as given by this theory is

$$
p - p_\infty = \frac{2q}{M} \left[\frac{1}{V} w_{,t} + w_{,x} + \frac{(\gamma + 1)}{4} M \left(\frac{1}{V} w_{,t} + w_{,x} \right)^2 \right.
$$
$$
\left. + \frac{(\gamma + 1)}{12} M^2 \left(\frac{1}{V} w_{,t} + w_{,x} \right)^3 \right] \qquad (4)
$$

The first two terms in the brackets in Eq. (4) constitutes the first-order piston theory aerodynamics and Eq. (4) without the cubic term represents the second-order piston theory aerodynamics.

In reference [9], McIntosh uses a modified form of Eq. (4). In his work, the $w_{,t}$ in the cubed parentheses is neglected. Since a complete derivation of the third-order piston aerodynamic theory would include this term, and since the additional complications to include this term in the finite element formulation is minimal, this term is retained. Retaining this term will allow for a full evaluation of it's influence on the panel's response.

Piston, Ackeret, and other quasi-steady aerodynamic theories have been shown [14] to give good estimates of the panel thickness required to prevent panel flutter. However, all of the references in the literature do strongly suggest that these theories are only valid for Mach number ranges greater than 1.6–2.0. Generally, this is taken to be greater than $\sqrt{2}$.

Three-Dimensional Rectangular Panel

For a general plate element undergoing both bending and extension, the complete strain, for any point through the thickness located at coordinate z, is composed of two parts. The first part is due to stretching the midsurface, and the second part is due

to the change in curvature, $\{\kappa\}$, during bending. Thus, using Kirchhoff hypothesis, the total strain can be written as

$$\{\epsilon\} = \{e\} + z\{\kappa\} = \left\{ \begin{array}{c} e_x \\ e_y \\ e_{xy} \end{array} \right\} + z \left\{ \begin{array}{c} \kappa_x \\ \kappa_y \\ \kappa_{xy} \end{array} \right\} \quad (5)$$

If the relationships between the strain-displacement in Eq. (3) are written as a vector, then the membrane strain, $\{e\}$, takes on the form

$$\{e\} = \left\{ \begin{array}{c} u_{,x} + \frac{1}{2}w_{,x}^2 \\ v_{,y} + \frac{1}{2}w_{,y}^2 \\ u_{,y} + v_{,x} + w_{,x}w_{,y} \end{array} \right\} \quad (6)$$

The membrane strains in Eq. (6) can also be written as

$$\{e\} = \{e_m\} + \{e_{mb}\} \quad (7)$$

where $\{e_m\}$ is the linear portion of the membrane strain and $\{e_{mb}\}$ is the nonlinear, von Karman, membrane-bending coupling strains. The curvatures written in terms of the transverse displacement, w, become

$$\{\kappa\} = \left\{ \begin{array}{c} -w_{,xx} \\ -w_{,yy} \\ -2w_{,xy} \end{array} \right\} \quad (8)$$

Proceeding from this point, the displacements in Eqs. (6) and (8) are approximated over a typical element using interpolation functions and nodal displacement quantities as follows:

$$\begin{aligned} w &= [\phi_w]\{\Delta w\} \\ u &= [\phi_u]\{\Delta u\} \\ v &= [\phi_v]\{\Delta v\} \end{aligned} \quad (9)$$

Using the Eqs. (6) and (8), the curvatures and midsurface strains, in the von Karman sense, are related to the nodal displacements as

$$\{\kappa\} = \left\{ \begin{array}{c} -w_{,xx} \\ -w_{,yy} \\ -2w_{,xy} \end{array} \right\} = \left[\begin{array}{c} -[\phi_w]_{,xx} \\ -[\phi_w]_{,yy} \\ -2[\phi_w]_{,xy} \end{array} \right] \{\Delta w\} \quad (10)$$

and for $\{e\} = \{e_m\} + \{e_{mb}\}$

$$\{e_m\} = \left[\begin{array}{cc} [\phi_u]_{,x} & 0 \\ 0 & [\phi_v]_{,y} \\ {[\phi_u]_{,y}} & [\phi_v]_{,x} \end{array} \right] \left\{ \begin{array}{c} \{\Delta u\} \\ \{\Delta v\} \end{array} \right\}$$

$$\{e_{mb}\} = \frac{1}{2} \left[\begin{array}{cc} w_{,x} & 0 \\ 0 & w_{,y} \\ w_{,y} & w_{,x} \end{array} \right] \left[\begin{array}{c} [\phi_w]_{,x} \\ {[\phi_w]_{,y}} \end{array} \right] \{\Delta w\} \quad (11)$$

The variation of the curvatures and midsurface strains are similarly related to the nodal displacements.

Using Eq. (1) result in the following matrix equation for the rectangular plate element:

$$\left[\begin{array}{cc} [m_f] & [0] \\ [0] & [m_m] \end{array} \right] \left\{ \begin{array}{c} \ddot{w}_f \\ \ddot{w}_m \end{array} \right\}$$

$$+ \left[\begin{array}{cc} ([g] + [g1_t] + [g2_{ft}] + [g2_t]) & [0] \\ [0] & [0] \end{array} \right] \left\{ \begin{array}{c} \dot{w}_f \\ \dot{w}_m \end{array} \right\}$$

$$+ \left[\begin{array}{cc} ([a] + [a1_t] + [a1_f] + [a2_{ft}] + [a2_f]) & [0] \\ [0] & [0] \end{array} \right] \left\{ \begin{array}{c} w_f \\ w_m \end{array} \right\}$$

$$+ \left[\begin{array}{cc} [k_{ff}] & [k_{Bfm}] \\ [k_{Bmf}] & [k_{mm}] \end{array} \right] \left\{ \begin{array}{c} w_f \\ w_m \end{array} \right\}$$

$$+ \left[\begin{array}{cc} [k1_{ff}] & [k1_{fm}] \\ [k1_{mf}] & [0] \end{array} \right] \left\{ \begin{array}{c} w_f \\ w_m \end{array} \right\} + \left[\begin{array}{cc} [k1_{Bff}] & [0] \\ [0] & [0] \end{array} \right] \left\{ \begin{array}{c} w_f \\ w_m \end{array} \right\}$$

$$+ \left[\begin{array}{cc} [k2_{ff}] & [0] \\ [0] & [0] \end{array} \right] \left\{ \begin{array}{c} w_f \\ w_m \end{array} \right\} = \left\{ \begin{array}{c} f_f \\ f_m \end{array} \right\} \quad (12)$$

where

$$\left\{ \begin{array}{c} \Delta w \\ \Delta u \\ \Delta v \end{array} \right\} = \left\{ \begin{array}{c} w_f \\ w_m \end{array} \right\} \quad (13)$$

and $\{f\}$ is the internal element equilibrium forces, $[k]$ is the linear elastic stiffness matrix, and $[k1]$ and $[k2]$ are nonlinear stiffness matrices which depend linearly and quadratically upon displacements, respectively.

The variation principle in Eq. (1) represents a finite element approach to study the limit-cycle oscillations of three-dimensional composite panels at hypersonic speeds. The third-order piston theory aerodynamics for the three-dimensional case will produce two linear aerodynamic influence matrices, $[g]$ and $[a]$, and seven nonlinear aerodynamic influence matrices, $[g1_t]$, $[g2_t]$, $[g2_{ft}]$, $[a1_t]$, $[a1_f]$, $[a2_{ft}]$, and $[a2_f]$, where the aerodynamic matrices are functions of the system aerodynamic parameters, in particular the dynamic pressure, q. The aerodynamic influence matrices $[g]$ and $[a]$ are linear, whereas $[g1_t]$, $[a1_t]$, and $[a1_f]$ depend linearly, denoted with 1, upon the displacements, denoted with subscript f, and/or the time derivative of the displacements (generalized velocities), denoted with subscript, t. The other four matrices, $[g2_{ft}]$, $[g2_t]$, $[a2_{ft}]$, and $[a2_f]$, are quadratic, denoted with 2, in displacement and/or generalized velocities. The symmetry in the first-order nonlinear stiffness matrix has been preserved [52] at the expense of transferring the nonlinearity $[k1_{fm}]$ into two equal parts and producing the $[k1_{ff}]$ term. A similar transformation was used in developing the $[k1_{Bff}]$ term. The aerodynamic damping matrices, $[g]$, $[g1]$ and $[g2]$ are symmetrical while the aerodynamic influence matrices, $[a]$, $[a1]$ and $[a2]$ are skew-symmetric.

SYSTEM FINITE ELEMENT FORMULATION AND SOLUTION PROCEDURE

In this section, a detailed description of the assembly procedure, solution procedure and computational methods that were developed to solve the large-amplitude panel flutter, using third-order piston aerodynamic theory, equations is presented.

System Finite Element Formulation

By sub-dividing the problem domain into a finite number of discrete elements, a subsystem of elements for the

three-dimensional panel can be assembled. Ensuing assembly of the elements, using the methods of references [53] and [54], the boundary conditions are imposed on the assembled system equation using the method outlined by Reddy [55]. The constrained system finite element equations are then available for an iterative solution.

After assembling the individual finite elements for the entire system and applying the kinematic boundary conditions (e.g., for simple, in-plane immovable supports; $u(0,y) = u(a,y) = v(x,0) = v(x,b) = w(0,y) = w(a,y) = w(x,0) = w(x,b) = 0$), the nonlinear equation of motion for the coupled (bending/membrane) system represents a finite element approach for solving the three-dimensional panel flutter problem. The convention that upper case matrix notation pertains to the assembled structure is used in this study to parallel the system and element formulations.

The constrained system equation for the three-dimensional rectangular panels has the following form:

$$
\begin{bmatrix} [M_f] & [0] \\ [0] & [M_m] \end{bmatrix} \begin{Bmatrix} \ddot{W}_f \\ \ddot{W}_m \end{Bmatrix} + \begin{bmatrix} ([G]+[G1_t]+[G2_t]+[G2_{ft}]) & [0] \\ [0] & [0] \end{bmatrix} \begin{Bmatrix} \dot{W}_f \\ \dot{W}_m \end{Bmatrix}
$$

$$
+ \begin{bmatrix} ([\mathcal{A}]+[A1_t]+[A1_f]+[A2_{ft}]+[A2_f]) & [0] \\ [0] & [0] \end{bmatrix} \begin{Bmatrix} W_f \\ W_m \end{Bmatrix}
$$

$$
+ \begin{bmatrix} [K_{ff}] & [K_{Bfm}] \\ [K_{Bmf}] & [K_{mm}] \end{bmatrix} \begin{Bmatrix} W_f \\ W_m \end{Bmatrix} + \begin{bmatrix} [K1_{ff}] & [K1_{fm}] \\ [K1_{mf}] & [0] \end{bmatrix} \begin{Bmatrix} W_f \\ W_m \end{Bmatrix}
$$

$$
+ \begin{bmatrix} [K1_{Bff}] & [0] \\ [0] & [0] \end{bmatrix} \begin{Bmatrix} W_f \\ W_m \end{Bmatrix} + \begin{bmatrix} [K2_{ff}] & [0] \\ [0] & [0] \end{bmatrix} \begin{Bmatrix} W_f \\ W_m \end{Bmatrix} = \begin{Bmatrix} 0 \\ 0 \end{Bmatrix} \tag{14}
$$

where $\{W_f\}$ and $\{W_m\}$ are the constrained nodal displacements of the assembled three-dimensional system.

Similar to the two-dimensional case [44], Eq. (14), as written, is a damped vibration problem in the configuration space; and as such, does not conform to standard eigenvalue solution algorithms. Thus, the approach of transforming the problem from the configuration space to a state space is used. By making the transformation to the state space, the governing matrix equation, Eq. (14), becomes

$$
\begin{bmatrix} [M] & [0] \\ [0] & [I] \end{bmatrix} \begin{Bmatrix} \overset{\circ}{\dot{W}} \\ W \end{Bmatrix} + \begin{bmatrix} [G] & [K] \\ [-I] & [0] \end{bmatrix} \begin{Bmatrix} \dot{W} \\ W \end{Bmatrix} = \{0\} \tag{15}
$$

where

$$
[M] = \begin{bmatrix} [M_f] & [0] \\ [0] & [M_m] \end{bmatrix} \tag{16}
$$

$$
[G] = \begin{bmatrix} ([G]+[G1_t]+[G2_t]+[G2_{ft}]) & [0] \\ [0] & [0] \end{bmatrix} \tag{17}
$$

$$
[K] = \begin{bmatrix} ([\mathcal{A}]+[A1_t]+[A1_f]+[A2_{ft}]+[A2_f]) & [0] \\ [0] & [0] \end{bmatrix}
$$
$$
+ \begin{bmatrix} [K_{ff}] & [K_{Bfm}] \\ [K_{Bmf}] & [K_{mm}] \end{bmatrix} + \begin{bmatrix} [K1_{ff}] & [K1_{fm}] \\ [K1_{mf}] & [0] \end{bmatrix}
$$
$$
+ \begin{bmatrix} [K1_{Bff}] & [0] \\ [0] & [0] \end{bmatrix} + \begin{bmatrix} [K2_{ff}] & [0] \\ [0] & [0] \end{bmatrix} \tag{18}
$$

$$
\{W\} = \begin{Bmatrix} W_f \\ W_m \end{Bmatrix} \tag{19}
$$

$$
\{\dot{W}\} = \begin{Bmatrix} \dot{W}_f \\ \dot{W}_m \end{Bmatrix} \tag{20}
$$

and $[I]$ is the identity matrix.

Linearizing Procedure

The solution procedure for the three-dimensional panel is fundamentally the same as ref. [44] where the solution to the homogeneous problem is sought in the form of

$$
\begin{Bmatrix} \dot{W} \\ W \end{Bmatrix} = \tilde{c} \begin{Bmatrix} \Phi_1 \\ \Phi_2 \end{Bmatrix} e^{\Omega t} \tag{21}
$$

where $\{\Phi_1\}$ and $\{\Phi_2\}$ are complex eigenvectors that are arranged as a single column vector, $\Omega = (\alpha + i\omega)$ is the complex eigenvalue, and $\tilde{c}$ is a nonzero (scalar) constant displacement amplitude. Substituting the assumed response into Eq. (15) results in the following eigenvalue problem:

$$
\tilde{c} \left(\Omega \begin{bmatrix} [M] & [0] \\ [0] & [I] \end{bmatrix} + \begin{bmatrix} [G] & [K] \\ [-I] & [0] \end{bmatrix} \right) \begin{Bmatrix} \Phi_1 \\ \Phi_2 \end{Bmatrix} e^{\Omega t} = \{0\} \tag{22}
$$

By expressing $e^{\Omega t}$ as a complex quantity in the Euler form and requiring both coefficients of $\sin(\omega t)$ and $\cos(\omega t)$ to vanish, then Eq. (22) can be written as two separate equations

$$
\tilde{c}\, e^{\alpha t} \left(\Omega \begin{bmatrix} [M] & [0] \\ [0] & [I] \end{bmatrix} + \begin{bmatrix} [G] & [K] \\ [-I] & [0] \end{bmatrix} \right) \begin{Bmatrix} \Phi_1 \\ \Phi_2 \end{Bmatrix} \cos(\omega t) = \{0\} \tag{23}
$$

$$
i\, \tilde{c}\, e^{\alpha t} \left(\Omega \begin{bmatrix} [M] & [0] \\ [0] & [I] \end{bmatrix} + \begin{bmatrix} [G] & [K] \\ [-I] & [0] \end{bmatrix} \right) \begin{Bmatrix} \Phi_1 \\ \Phi_2 \end{Bmatrix} \sin(\omega t) = \{0\} \tag{24}
$$

Since $\tilde{c}$ is nonzero, Eq. (22) is for the constrained system, and the solution sought is for all times greater than zero, both Eqs. (23) and (24) represent the same eigenvalue problem. To solve Eq. (23) or (24), the nonlinear matrices in Eq. (14) need to be evaluated. Also, since all of the system quantities used in developing these equations are real, it must be concluded that the nodal response quantities must also be real [1]. The field expressions for the transverse panel displacement, velocity, and slope are given in Eq. (9). All of these quantities can be approximated from Eq. (21) by normalizing the eigenvector as follows and recognizing that $\{W\}$ is a real quantity, and as such take only the real part of the normalized Eq. (21)

$$
\begin{Bmatrix} \dot{W} \\ W \end{Bmatrix} = \frac{\tilde{c}\, e^{\alpha t}}{|(\Phi_2)_k|} \begin{Bmatrix} |\Phi_1| & \cos(\beta - \beta_k) \\ |\Phi_2| & \cos(\beta - \beta_k) \end{Bmatrix} \cos(\omega t) \tag{25}
$$

The quantity $|(\Phi_2)_k|$ is the magnitude of the largest transverse displacement component of the eignevector that corresponds to $\{\Phi_2\}$, and β_k is the corresponding phase angle. Next, denote $c = \tilde{c}\, e^{\alpha t}$ as the damped amplitude. Thus, it is clear from Eq. (25) that the sign of the real part of the eigenvalue controls the stability of the solution. The solution is stable for all α that are less than zero. For α equal to zero, then c equals $\tilde{c}$ and the resulting solution corresponds to that of a limit-cycle oscillation. By letting

$$
\begin{Bmatrix} \bar{\Phi}_1 \\ \bar{\Phi}_2 \end{Bmatrix} = \frac{1}{|(\Phi_2)_k|} \begin{Bmatrix} |\Phi_1| \cos(\beta - \beta_k) \\ |\Phi_2| \cos(\beta - \beta_k) \end{Bmatrix} \tag{26}
$$

then Eq. (25) becomes,

$$
\begin{Bmatrix} \dot{W} \\ W \end{Bmatrix} = c \begin{Bmatrix} \bar{\Phi}_1 \\ \bar{\Phi}_2 \end{Bmatrix} \cos(\omega t) \tag{27}
$$

Using Eqs. (27), and (9) the (scalar magnitude) transverse velocities and slopes become

$$w(x,y,t)_{,t} = [\phi_w] \left\{ \bar{\Phi}_{1f} \right\}_j \cos(\omega t)$$

$$w(x,y,t)_{,x} = [\phi_w]_{,x} \left\{ \bar{\Phi}_{2f} \right\}_j \cos(\omega t)$$

$$w(x,y,t)_{,y} = [\phi_w]_{,y} \left\{ \bar{\Phi}_{2f} \right\}_j \cos(\omega t)$$

$$u(x,y,t)_{,x} = [\phi_u]_{,x} \left\{ \bar{\Phi}_{2m} \right\}_j \cos(\omega t) \qquad (28)$$

$$u(x,y,t)_{,y} = [\phi_u]_{,y} \left\{ \bar{\Phi}_{2m} \right\}_j \cos(\omega t)$$

$$v(x,y,t)_{,x} = [\phi_v]_{,x} \left\{ \bar{\Phi}_{2m} \right\}_j \cos(\omega t)$$

$$v(x,y,t)_{,y} = [\phi_v]_{,y} \left\{ \bar{\Phi}_{2m} \right\}_j \cos(\omega t)$$

In Eq. (28), the column vectors $\left\{ \bar{\Phi}_1 \right\}_j$ and $\left\{ \bar{\Phi}_2 \right\}_j$ contain the appropriate global eigenvector quantities from $\left\{ \bar{\Phi}_1 \right\}$ and $\left\{ \bar{\Phi}_2 \right\}$ that correspond to the particular j-th finite element. The three-dimensional vector $\left\{ \bar{\Phi}_{1f} \right\}_j$ uses the subscript "f" or "m" to denote the appropriate bending or membrane quantity that correspond to the particular j-th finite element, respectively. Thus, with Eq. (27), the nonlinear terms in Eq. (23) can be evaluated. By making use of trigonometric identities for $\cos^2(wt)$ and $\cos^3(wt)$, and neglecting the second and third harmonics, the following approximations may be used to linearize Eq. (23):

$$\cos^2(\omega t) \approx \frac{\sqrt{2}}{2} \cos(\omega t)$$

$$\cos^3(\omega t) \approx \frac{3}{4} \cos(\omega t) \qquad (29)$$

The various linearizing methods, [37]–[43], that have been used in the past have bounded these values. From Eq. (28), the time functions have an absolute value range from zero to one. The lower value of zero will reduce the nonlinear problem to a linear one while the upper limit of one would calculate the nonlinear stiffness based on the maximum deflected configuration. The lower (linear) limit as discussed in the introduction merely defines the flutter boundary as an instability. The upper limit defines an over-stiff system by assuming the maximum value of the developed midsurface force to occur over the entire cycle. Physically, the actual value starts at zero then progresses to the maximum value of one then back to zero over a half-cycle and then repeated through the second half-cycle. Thus, neglecting the second and third harmonics in Eq. (28) will predict a solution that is clearly bounded between the physical extremes. In fact, the value, $\frac{\sqrt{2}}{2}$, is exactly the root-mean-square value of a harmonic function over its period, and $\frac{3}{4}$ is in the same range.

Using Eqs. (27) and (29), the nonlinear Eq. (12) for the three-dimensional panel result in the following element equations:

stiffness $\qquad\qquad (30)$

$$[k1_{fm}] = c[k1_{fm}] \cos(\omega t) \qquad (30a)$$

$$[k1_{mf}] = c[k1_{mf}] \cos(\omega t) \qquad (30b)$$

$$[k1_{ff}] = c[k1_{ff}] \cos(\omega t) \qquad (30c)$$

$$[k1_{Bff}] = c[k1_{Bff}] \cos(\omega t) \qquad (30d)$$

$$[k2_{ff}] = c^2[k2_{ff}] \cos^2(\omega t) \qquad (30e)$$

aerodynamic influence $\qquad\qquad (31)$

$$[g1_t] = c[g1_t] \cos(\omega t) \qquad (31a)$$

$$[g2_t] = c^2[g2_t] \cos^2(\omega t) \qquad (31b)$$

$$[g2_{ft}] = c^2[g2_{ft}] \cos^2(\omega t) \qquad (31c)$$

$$[a1_t] = c[a1_t] \cos(\omega t) \qquad (31d)$$

$$[a1_f] = c[a1_f] \cos(\omega t) \qquad (31e)$$

$$[a2_{ft}] = c^2[a2_{ft}] \cos^2(\omega t) \qquad (31f)$$

$$[a2_f] = c^2[a2_f] \cos^2(\omega t) \qquad (31g)$$

The linearized stiffness and aerodynamic influence matrices are defined as follows using the definitions:

$$[C_\theta] = \begin{bmatrix} [\phi_w]_{,x} \\ [\phi_w]_{,y} \end{bmatrix} \qquad (32)$$

$$[P_w] = \begin{bmatrix} -[\phi_w]_{,xx} \\ -[\phi_w]_{,yy} \\ -2[\phi_w]_{,xy} \end{bmatrix} \qquad (33)$$

$$[P_u] = \begin{bmatrix} [\phi_u]_{,x} & 0 \\ 0 & [\phi_v]_{,y} \\ [\phi_u]_{,y} & [\phi_v]_{,x} \end{bmatrix} \qquad (34)$$

$$[\Theta] = \begin{bmatrix} [\phi_w]_{,x} \left\{ \bar{\Phi}_{2f} \right\}_j & 0 \\ 0 & [\phi_w]_{,y} \left\{ \bar{\Phi}_{2f} \right\}_j \\ [\phi_w]_{,y} \left\{ \bar{\Phi}_{2f} \right\}_j & [\phi_w]_{,x} \left\{ \bar{\Phi}_{2f} \right\}_j \end{bmatrix} \qquad (35)$$

The linearized midsurface forces,

$$\left\{ \mathcal{N}_A \right\} = [A][P_u] \left\{ \bar{\Phi}_{2m} \right\}_j \qquad (36)$$

and

$$\left\{ \mathcal{N}_B \right\} = [B][P_w] \left\{ \bar{\Phi}_{2f} \right\}_j \qquad (37)$$

where

$$\left\{ \mathcal{N}_A \right\} = \left\{ \begin{array}{c} \mathcal{N}_{Ax} \\ \mathcal{N}_{Ay} \\ \mathcal{N}_{Axy} \end{array} \right\} \qquad (38)$$

and

$$\left\{ \mathcal{N}_B \right\} = \left\{ \begin{array}{c} \mathcal{N}_{Bx} \\ \mathcal{N}_{By} \\ \mathcal{N}_{Bxy} \end{array} \right\} \qquad (39)$$

are used to define $[\mathcal{N}_A]$ and $[\mathcal{N}_B]$ as

$$\begin{bmatrix} \mathcal{N}_{Ax} & \mathcal{N}_{Axy} \\ \mathcal{N}_{Axy} & \mathcal{N}_{Ay} \end{bmatrix} = [\mathcal{N}_A] \qquad (40)$$

$$\begin{bmatrix} \mathcal{N}_{Bx} & \mathcal{N}_{Bxy} \\ \mathcal{N}_{Bxy} & \mathcal{N}_{By} \end{bmatrix} = [\mathcal{N}_B] \qquad (41)$$

linearized stiffness $\qquad\qquad (42)$

$$[k1_{mf}] = \frac{1}{2} \int_S [P_u]^T [A][\Theta][C_\theta] dS \qquad (42a)$$

$$[k2_{ff}] = \frac{1}{2} \int_S [C_\theta]^T [\Theta]^T [A][\Theta][C_\theta] dS \qquad (42b)$$

$$[k1_{Bff}] = \frac{1}{2} \int_S \left([C_\theta]^T [\mathcal{N}_B][C_\theta] + [C_\theta]^T [\Theta]^T [B][P_w] \right.$$

$$\left. + [P_w]^T [B][\Theta][C_\theta] \right) dS \qquad (42c)$$

$$[k1_{fm}] = \frac{1}{2} \int\limits_S [C_\theta]^T [\Theta]^T [A][P_u] dS \qquad (42d)$$

$$[k1_{ff}] = \frac{1}{2} \int\limits_S [C_\theta]^T [\mathcal{N}_A][C_\theta] dS \qquad (42e)$$

linearized aerodynamic influence (43)

$$[g1_t] = \frac{q(\gamma+1)}{2V^2} \int\limits_S \left([\phi_w] \{\bar{\Phi}_{1f}\}_j \right) \{\phi_w\}[\phi_w] dS \qquad (43a)$$

$$[g2_t] = \frac{q(\gamma+1)M}{6V^3} \int\limits_S \left([\phi_w] \{\bar{\Phi}_{1f}\}_j \right)^2$$
$$\times \{\phi_w\}[\phi_w] dS \qquad (43b)$$

$$[g2_{ft}] = \frac{q(\gamma+1)M}{2V^2} \int\limits_S \left([\phi_w]_{,x} \{\bar{\Phi}_{2f}\}_j \right)$$
$$\times \left([\phi_\omega] \{\bar{\Phi}_{1f}\}_j \right) \{\phi_w\}[\phi_w] dS \qquad (43c)$$

$$[a1_t] = \frac{q(\gamma+1)}{V} \int\limits_S$$
$$\times \left([\phi_w] \{\bar{\Phi}_{1f}\}_j \right) \{\phi_w\}[\phi_w]_{,x} dS \qquad (43d)$$

$$[a1_f] = \frac{q(\gamma+1)}{2} \int\limits_S$$
$$\times \left([\phi_w]_{,x} \{\bar{\Phi}_{2f}\}_j \right) \{\phi_w\}[\phi_w]_{,x} dS \qquad (43e)$$

$$[a2_{ft}] = \frac{q(\gamma+1)M}{2V} \int\limits_S \left([\phi_w]_{,x} \{\bar{\Phi}_{2f}\}_j \right)$$
$$\times \left([\phi_\omega] \{\bar{\Phi}_{1f}\}_j \right) \{\phi_w\}[\phi_w]_{,x} dS \qquad (43f)$$

$$[a2_f] = \frac{q(\gamma+1)M}{6} \int\limits_S \left([\phi_w]_{,x} \{\bar{\Phi}_{2f}\}_j \right)^2$$
$$\times \{\phi_w\}[\phi_w]_{,x} dS \qquad (43g)$$

where $(\ )_{,x} = \frac{\partial(\ )}{\partial x}$.

Linearizing Method for System Equations

Assembling the element equations for the constrained system and using the linearized element matrices, Eqs. (42) and (43), results in the following linearized eigenvalue problem:

$$\bar{c}\, e^{\alpha t} \left(\Omega \begin{bmatrix} [\mathcal{M}] & [0] \\ [0] & [I] \end{bmatrix} + \begin{bmatrix} [\mathcal{G}] & [\mathcal{K}] \\ [-I] & [0] \end{bmatrix} \right) \begin{Bmatrix} \Phi_1 \\ \Phi_2 \end{Bmatrix} \cos(\omega t) = \{0\} \qquad (44)$$

where the linearized matrices $[\mathcal{G}]$ and $[\mathcal{K}]$ are defined for the three-dimensional panel as

$$[\mathcal{M}] = \begin{bmatrix} [M_f] & [0] \\ [0] & [M_m] \end{bmatrix} \qquad (45)$$

$$[\mathcal{G}] = \begin{bmatrix} \left([G] + \frac{\sqrt{2}}{2} c[\mathrm{G}1_t] + \frac{3}{4}c^2[\mathrm{G}2_t] + \frac{3}{4}c^2[\mathrm{G}2_{ft}] \right) & [0] \\ [0] & [0] \end{bmatrix} \qquad (46)$$

$$[\mathcal{K}] = \begin{bmatrix} \left([A] + \frac{\sqrt{2}}{2}(c)[\mathrm{A}1_t] + \frac{\sqrt{2}}{2}(c)[\mathrm{A}1_f] + \frac{3}{4}(c)^2[\mathrm{A}2_{ft}] + \frac{3}{4}(c)^2[\mathrm{A}2_f] \right) & [0] \\ [0] & [0] \end{bmatrix}$$
$$+ \begin{bmatrix} [K_{ff}] & [K_{Bfm}] \\ [K_{Bmf}] & [K_{mm}] \end{bmatrix} + \frac{\sqrt{2}}{2}(c) \begin{bmatrix} [\mathrm{K}1_{ff}] & [\mathrm{K}1_{fm}] \\ [\mathrm{K}1_{mf}] & [0] \end{bmatrix}$$
$$+ \frac{\sqrt{2}}{2}(c) \begin{bmatrix} [\mathrm{K}1_{Bff}] & [0] \\ [0] & [0] \end{bmatrix} + \frac{3}{4}(c)^2 \begin{bmatrix} [\mathrm{K}2_{ff}] & [0] \\ [0] & [0] \end{bmatrix} \qquad (47)$$

A detailed look at the nonlinear problem from the physical viewpoint indicates that what is required, is to find a deflected shape in order to compute the eigenvalues. Since the eigenvectors are related to the deflected shape, all that is needed to approximate the solution is a shape that satisfies the geometric (essential) boundary conditions and is a variation of the exact shape. The first approximation is the normalized linear flutter mode shape of interest. Further refinements are made by using the normalized nonlinear mode shape as an estimate of the deflected shape. This can be repeated until the estimated deflected shape and the computed normalized eigenvector differ by as small a value as required. This solution procedure can best be described as a linearized updated mode with a nonlinear time function approximation (LUM/NTF) method [44].

Solution Procedure

If Eq. (21) is normalized, then it can be scaled to a given limit-cycle amplitude c. Having normalized and scaled Eq. (21), then Eq. (26) results, and u, v, w and their derivatives for each element can be easily computed as shown in Eq. (28). Thus, by dropping the nonlinear terms in Eq. (22) and solving the linear eigenvalue problem, the first estimate of the nodal quantities can be approximated. With the linear eigenvectors, the process just described can be used to approximate the quantities necessary to assemble the linearized element matrices and the assembled constrained system matrices. The same process can be repeated until successive iterations yield the same eigenevalues, both real and imaginary, and the same eigenvectors within the limits of a convergence criterion [56]. Therefore, for a given panel configuration and dynamic pressure, the nonlinear system eigenvalues and eigenvectors can be computed.

As the dynamic pressure is increased monotonically from zero ($\lambda = 0$ corresponds to in-vacuo large-amplitude free vibration), the symmetric, real and positive-definite stiffness matrix is perturbed by the skewed aerodynamic-influence matrix so that two of the eigenvalues approach each other until they coalesce. A critical dynamic pressure, λ_{cr}, for the linear structure ($c/h = 0$) and a limit-cycle dynamic pressure, λ_ℓ, for the nonlinear structure ($c/h \neq 0$) are determined when the real part of one of the eigenvalues approaches positive values [44, 57] for a fixed dynamic pressure.

VERIFICATION OF FINITE ELEMENT METHOD

All numerical results are using a rectangular plate element where the transverse displacement function, w, is a bi-cubic polynomial in x and y, and the membrane displacement functions, u and v, are bi-linear in x and y.

Flutter with Linear Aerodynamics—Isotropic

To establish confidence in the present solution method, Dowell's [18] well known numerical integration results along with Eslami's [32] harmonic balance solution for a simply supported, in-plane immovable, square panel are presented in Table 3. Since

both of these investigators display their limit-cycle results in the form of plots, the limit-cycle data shown in the table were read from their figures. The finite element results compare favorably with the maximum difference of only .2%. Also shown in Table 3 are the limit-cycle results for the clamped, in-plane immovable panel. Kuo et al. [21] and Eslami's [32] limit-cycle six-mode perturbation results were also evaluated from charts and compared within 1.8%.

Flutter with Linear Aerodynamics—Composite

A comparison to validate the present finite element method and solution procedure is made for a single layer anisotropic square panel. This panel is clamped along one edge parallel to the free stream flow with the other three edges free. This comparison combines the flutter phenomena with the full anisotropic material effects along with a mixed set of boundary conditions. The present finite element results for the critical dynamic pressure for three lamination angles are presented in Table 4. Since reference [58] elected to use a 5×5 mesh, these results are also for a 5×5 mesh. The information presented in Table 4 is for a slightly different definition of the nondimensional dynamic pressure which is noted in the table; thus, the values are smaller than those normally presented for a similar isotropic panel. For all three lamination angles that were evaluated, the present finite element method agreement is good.

NONLINEAR PANEL FLUTTER RESULTS

For the three-dimensional isotropic/composite panels, the finite element method has been employed to provide a full evaluation of the effects of the complete third-order piston aerodynamic theory. Several cases are presented that assess the influence of each of the higher-order terms. In addition, an evaluation of the composite panel effects is offered to investigate the influence of material orthotropy, number of layers, and stacking sequence. All of the material properties used in this section are from Ref. [60] and are summarized in Table 2.

An effort has been made to present finite element results for as many of the three-dimensional parameters as possible. Since for the two-dimensional panel [44], a range of $\frac{\mu}{M} = .01-0.1$ and $\frac{Mh}{a} = .05-0.1$ flow parameters were presented, the finite element results for the three-dimensional panel are provided for $\frac{\mu}{M} = .1$ and $\frac{Mh}{a} = .05$. Limiting the flow parameters for the three-dimensional panels minimizes the total number of complete system parameters necessary to study the flutter of composite panels. In addition, unless specifically noted the results presented in this study are for a square, simply-supported 8×4 half-plate symmetric mesh.

Limit-Cycle Oscillations

Panel flutter designs are generally focused on fatigue life (or service life) considerations. That is, the repeated cyclic application of a self-excited loading to a stress level in excess of the material's endurance limit results in a finite number of these applications before a structural failure/damage becomes emanate. Since the aerodynamic damping forces are nonlinear and amplitude-dependent, a stationary motion is achieved in which the panel gains energy during part of the cycle and dissipates energy during the remaining part of the cycle, so that during each cycle the net energy exchange is zero. Thus at a given flow velocity (dynamic pressure), the flow and the structure interact to produce a stable repeated oscillation at a specific amplitude and frequency. This stable repeated motion is known as a limit-cycle.

This study presents the numerical results necessary to develop a description of the limit-cycle flutter of a composite panel.

The orthotropic, simply supported, square panel ($a = 12$ in, $h = 0.04$ in) used for this first study is a single layer of boron aluminum, B/Al B5.6/Al—material 3, Table 2. Solving only the linear portion of Eq. (44) and varying the dynamic pressure from zero monotonically results in a variation of the system frequencies. As shown in Fig. 1, the eigenvalues of the first mode and third mode increase while the second and fourth mode decrease until two of the eigenvalues coalesce. For this configuration, the first and second eigenvalues coalesce; however, with aerodynamic damping present, the real part of the system eigenvalue vanishes at a slightly higher dynamic pressure. When the real part of the eigenvalue vanishes the associated value of the dynamic pressure is, for the linear analysis, referred to as the critical dynamic pressure and defines the stability boundary. The nondimensional dynamic pressure shown in Fig. 1 is defined as

$$\lambda = \frac{2qa^3}{MD_c} \quad (48)$$

where

$$D_c = E_{11}h^3 \quad (49)$$

The nondimensional λ for this study has a different definition than that which is usually used for isotropic materials. This definition of the dynamic pressure will be employed when presenting or discussing three-dimensional panels whether isotropic or composite.

By including the nonlinear effects (geometric and aerodynamic) in Eq. (44) for a fixed displacement amplitude and repeating the same analysis process, the value of λ for which the real part of the eigenvalue vanishes is found to occur at a larger dynamic pressure. For both a $c/h = +1.0$ and $c/h = -1.0$ amplitude ratio, the dynamic pressure and eigenvalue variations are shown in Fig. 2. As was the case for the two-dimensional panel [9, 44], the response is different for a positive or negative displacement amplitude. When the real part of the eigenvalue vanishes for a fixed displacement amplitude, the corresponding dynamic pressure is the limit-cycle dynamic pressure. Associated with this dynamic pressure and amplitude is the frequency at which the panel will oscillate.

Figure 2 shows the panel response for a fixed amplitude ratio. If this approach is repeated for several amplitude ratios, then the response shown in Fig. 3 results. These results show that as the limit-cycle dynamic pressure is increased above the critical value, then the panel will oscillate at increasing amplitude levels.

The typical panel limit-cycle deflection shape is shown in Fig. 4 for a full 12×8 finite element mesh; these results are plotted along the lines $y/b = 0.5$ and $x/a = .75$. The basic shape remains similar to those for two-dimensional panels. Similarly, the maximum panel deflection is noted to occur at .75 of the length.

Laminated Panel Effects

Since the stiffness of a laminate depends substantially on the number and orientation of each lamina in the laminate, an evaluation of a regular cross-ply laminated panel was performed. This evaluation computed the limit-cycle dynamic pressure for a range of limit-cycle amplitudes for several regular laminates. To effect this, a panel thickness was selected and the number of layers were increased from one to six as the limit-cycle amplitude was varied from zero to positive one plate thickness. As each new lamina was added to the laminate, the orientation was alternated between 0° and 90°. This results in a laminate that alternates between symmetric and unsymmetric; thus, for the unsymmetric laminate the bending-extension [B] matrix is non-zero. However, the [B] matrix is diagonal and only a 8×4-mesh half-plate was modeled to exploit global symmetry. The variation of the limit-cycle amplitude for a six-layer cross-ply laminate is shown in

Fig. 5. It is noted that the stiffer response is characterized by a single-layer orthotropic laminate, [0], and the softest response is exhibited by a two-layer, unsymmetric laminate, [0/90], with the 0's on the air flow side. This is to be expected since the two-layer cross-ply has an equal number of 0's and 90's, 50% of each. At three layers, the total percentage of 0's increase to 67%, the maximum percentage for a cross-ply. Any further increase in layers will reduce the effective stiffness of the laminate up to approximately six layers at which point it is noted that the response is no longer sensitive to the addition of alternating layers.

To further investigate the effects of lamination angle, a single layered laminate was evaluated. The lamination angle was varied from 0° to 90° and the limit-cycle dynamic pressure, for a fixed limit-cycle amplitude of 0.6 of the panel thickness, was computed. The variation of the lamination angle and its effect on the dynamic pressure is shown in Fig. 6. These results show that, again, the orthotropic laminate exhibits the most stable response. The difference between the 0° and 90° laminate is approximately a 20% reduction (for material 3) in the limit-cycle dynamic pressure changing more noticeably between 30° to 60°.

Boundary Support and Aspect Ratio Effects

As was noted in the introduction, all of the classical solution methods are for either simply supported or clamped supported panels. With the finite element method, any combination of support conditions is easy to accommodate. The limit-cycle results presented in Fig. 7 show the varying response that changing the support conditions has on panel flutter. These results indicate that the clamped panel resists flutter much better than the simply supported panel. It is interesting to note that the slopes for the various boundary support conditions behave according to the trailing edge support conditions.

Since most of these results were for a square panel, the effect of different aspect ratios ($a/b = 0.5$, 1.0, and 2.0) is shown in Fig. 8. The larger aspect ratios produce a more stable response, and the smaller the aspect ratio, the less stable the response. However, for an aspect ratio of $a/b = 0.5$, the loss in stability is not as great as the increase in stability for $a/b = 2.0$. Thus, for the same panel flow area, the most effective use of the material is to configure the geometry such that the flow-direction dimension is greater than the width.

Influence of Orthotropic Materials

The major portion of this study on three-dimensional panel flutter has focused on a single composite material. The orthotropic material was boron aluminum, B/Al, B5.6/Al— material 3, Table 2. For the materials listed in Table 2, it is easy to see that there are a considerable number of cases and conditions to evaluate in order to fully characterize flutter of a composite panel. This section attempts to address an approach to assess the panel fluttered for different composite materials. By defining a composite material parameter, $(\bar{E}_{11}E_{22}/G_{12}^2)\,\nu_{12}$, the critical ($c/h = 0$) and limit-cycle ($c/h \neq 0$) dynamic pressures can be scaled and plotted against this material parameter for several limit-cycle amplitudes. The results shown in Fig. 9 show a strong linear correlation of these parameters. Thus, given any new material properties, a reasonable estimate of the limit-cycle response can be assessed provided the analysis has been performed for at least two material systems. Further works is required in this area to provide the designer with a meaningful tool to accommodate flutter constraints into flow surface structural designs.

Nonlinear Aerodynamic Effects

To complete this study an assessment of the third-order piston aerodynamic theory is provided. The influence that the nonlinear aerodynamic terms have on the motion of the panel as it oscillates at a higher dynamic pressure is investigated for an isotropic material and two composite material stacking sequences. By including a small parameter multipler on each of the terms in the piston theory expression, then Eq. (4) can be written as

$$
p - p_\infty = \frac{2q}{M} \left[\frac{1}{V}\pi_{1t}\,w_{,t} + \pi_{1x}w_{,x} + \frac{(\gamma+1)}{4}M(\frac{1}{V}\pi_{2t}w_{,t} \right.
$$
$$
\left. + \pi_{2x}w_{,x})^2 + \frac{(\gamma+1)}{12}M^2(\frac{1}{V}\pi_{3t}w_{,t} \right.
$$
$$
\left. + \pi_{3x}w_{,x})^3 \right] \tag{50}
$$

where the parameter π can be varied for zero to one independently. Tables 5 and 6 summarize, for the parameters shown, a comparison of the limit-cycle results and the effects of neglecting each of the nonlinear terms independently of the others. The composite material results shown are for a boron aluminum material, B/Al B5.6/Al—material 3, Table 2. Seven cases were studied where the π parameters took on values of either zero or one. For all of these results, the term that has the most significant influence when included in Eq. (50) is the π_{2x} parameter. This is easily seen by noting the case 3 results in Tables 5 and 6. For this case, the first-order theory is used and only the π_{2x} parameter is nonzero. The most interesting conclusion from these results is that nearly all of the contribution from the nonlinear aerodynamics is contained in the $w_{,x}^2$ term.

SUMMARY AND CONCLUSIONS

The unsteady, hypersonic, aerodynamic theory and the von Karman large deflection plate theory were employed to formulate the aeroelastic problem. Nonlinear flutter analyses were performed to assess the influence of the higher-order aerodynamic theory on the structure's limit-cycle amplitude and the dynamic pressure of the flow velocity. The presented procedure has been used to solve the nonlinear panel flutter finite element equations. This procedure utilizes a linearized updated mode approach with a nonlinear time function approximation (LUM/NTF) method. Linear finite-element flutter for isotropic and composite panels and large amplitude isotropic panel flutter results were compared with existing classical solutions and excellent agreement between the proposed finite element method and alternate solution methods was found. The large amplitude panel flutter results using a frequency domain solution and the full third-order piston aerodynamic theory were presented to assess the influence of the nonlinear aerodynamic theory and for the cases investigated only the $w_{,x}^2$ term was found to be significant.

REFERENCES

1. Dungundji, J., "Theoretical Considerations of Panel Flutter at High Supersonic Mach Numbers," *AIAA J.*, Vol. 4, July 1966, pp. 1257–1266.

2. Dowell, E. H., "Panel Flutter: A Review of the Aeroelastic Stability of Plates and Shells," *AIAA J.*, Vol. 8, March 1970, pp. 385–399.

3. Reed, W. H., Hanson, P. W. and Alford, W. J., "Assessment of Flutter Model Testing Relating to the National Aerospace Plane," NASP Contractor Report 1002, 1987.

4. Laurenson, R. M. and McPherson, J. I., "Design Procedures for Flutter-Free Surface Panels," NASA CR-2801, 1977.

5. Cunningham, H. J., "Flutter Analysis of Flat Rectangular Panels Based on Three-Dimensional Supersonic Potential Flow," *AIAA J.*, Vol. 1, No. 8, August 1963, pp. 1795–1801.

6. Ashley, H. and Zartarian, G., "Piston Theory—A New Aerodynamic Tool for the Aeroelastician," *Journal of the Aeronautical Science*, Vol. 23, No. 12, December 1956.

7. Dowell, E. H., *Aeroelasticity of Plates and Shells*, Noordhoff International Publishing, Lyden, The Netherlands, 1975.

8. Woinowsky-Krieger, S., "The Effects of Axial Force on the Vibration of Hinged Bars," *Journal of Applied Mechanics*, Vol. 17, 1950, pp. 35–36.

9. McIntosh, S. G., Jr., "Theoretical Considerations of Some Nonlinear Aspects of Hypersonic Panel Flutter," Final Report, September 1, 1965 to August 31, 1970, NASA Grant NGR 05-020-102, Department of Aeronautics and Astronautics, Stanford University, Stanford, CA., 1970.

10. Bolotin, V. V., *Nonconservative Problems of the Theory of Elastic Stability*, McMillan Co., New York, 1963, pp. 199–312.

11. Fung, Y. C., "On Two-Dimensinal Panel Flutter," *Journal of the Aeronautical Sciences*, Vol. 25, March 1958, pp. 145–160.

12. Houbolt, J. C., "A Study of Several Aerothermoelastic Problems of Aircraft Structures in High-Speed Flight," Ph.D. Thesis, Mitteilung aus dem Institute fur Flugzeugstatik und Leuchbau, Nr. 5, E.T.H., Zurich, 1958.

13. Eisely, J. G., "The Flutter of a Two-Dimensional Buckled Plate with Clamped Edges in a Supersonic Flow," OSR-TN-56-296, July 1956.

14. Cunningham, H. J., "Flutter Analysis of Flat Rectangular Panels Based on Three-Dimensional Supersonic Unsteady Potential Flow," NASA TR R-256, 1967.

15. Fralich, R. W., "Postbuckling Effects on the Flutter of Simply Supported Rectangular Panels at Supersonic Speed," NASA TN D-1615, March 1965.

16. Dowell, E. H., "Nonlinear Oscillation of a Fluttering Plate II," *AIAA J.*, Vol. 5, No. 10, October 1967, pp. 1856–1862.

17. Dowell, E. H., and Voss, H. M., "Experimental and Theoretical Panel Flutter Studies in Mach Number Range 1.0 to 5.0," *AIAA J.*, Vol. 3, No. 12, December 1965, pp. 2292–2304.

18. Dowell, E. H., "Nonlinear Oscillation of a Fluttering Plate I," *AIAA J.*, Vol. 4, No. 7, July 1966, pp. 1267–1275.

19. Ventres, C. S., "Nonlinear Flutter of Clamped Plates," Ph.D. Dissertation, Princeton University, 1970.

20. Kobayashi, S., "Flutter of Simply-Supported Rectangular Panels in a Supersonic Flow—Two-Dimensional Panel Flutter, I—Simply-Supported Panel, II—Clamped Panel," *Transaction of Japan Society of Aeronautical and Space Sciences*, Vol. 5, 1962, pp. 79–118.

21. Kuo, C. C., Morino, L., and Dungundji, J., "Perturbation and Harmonic Balance for Treating Nonlinear Panel Flutter," *AIAA J.*, Vol. 10, Nov. 1972, pp. 1470–1484.

22. Eastep, F. E., and McIntosh, S. C., "The Analysis of Nonlinear Panel Flutter and Response Under Random Excitation or Nonlinear Aerodynamic Loading," AIAA/ASME 11th Structural Dynamics, and Materials Conference, Denver, CO, April 22-24, 1970, pp. 36–47.

23. Eastep, F. E., "Nonlinear Oscillations of Elastic Panel in a Supersonic Nonviscous Airstream," SUDAAR No. 354, Dept. of Aeronautics and Astronautics, Stanford University, Stanford, CA, August 1968.

24. Morino, L., "A Perturbation Method for Treating Nonlinear Panel Flutter Problems," *AIAA J.*, Vol. 7, March 1969, pp. 405–410.

25. Morino, L. and Kuo, C. C., "Detailed Extensions of Perturbation Methods for Nonlinear Panel Flutter," ASRL TR 164-2, M.I.T., Cambridge, MA, March 1971.

26. Perlmutter, A. A., "On the Aeroelastic Stability of Orthotropic Panels in Supersonic Flow," *Journal of AeroSpace Science*, Vol. 29, November 1962, pp. 1332–1338.

27. Calligeros, J. M. and Dungundji, J., "Supersonic Flutter of Rectangular Orthotropic Panels with Arbitrary Orientation of the Orthotropicity," AFOSR5328, June 1963.

28. Ketter, D. J., "Flutter of Flat Rectangular, Orthotropic Panels," *AIAA J.*, Vol. 1, February 1966, pp. 116–124.

29. Shyprykevich, P. and Sawyer, J. W., "Orthotropic Panel Flutter at Arbitrary Yaw Angles-Experiment and Correlation with Theory." *AIAA J.*, Paper 73-192, January 1973.

30. Oyibo, G. A., "Flutter of Orthotropic Panels in Supersonic Flow Using Affine Transformation," *AIAA J.*, Vol. 21, February 1983, pp. 283–289.

31. Librescu, L., "Aeroelastic Stability of Orthotropic Heterogeneous Thin Panels in the Vicinity of Flutter Critical Boundary," *Journal de Mechanique*, 4, 1965, pp. 51–76.

32. Eslami, H., "Nonlinear Flutter and Forced Oscillations of Rectangular Symmetric Cross-Ply and Orthotropic Panels Using Harmonic Balance and Perturbation Method," Ph.D. Dissertation, Old Dominion University, Norfolk, VA, 1987.

33. Eslami, H. and Ibrahim, S. R., "Nonlinear Flutter of Specially Orthotropic Laminated Panels," Proceedings of 27th Structures, Structural Dynamics and Materials Conference, San Antonio, TX, 1986, pp. 393–302.

34. Olson, M. D., "Finite Element Approach to Panel Flutter," *AIAA J.*, Vol. 5, December 1967, pp. 2267–2270.

35. Olson, M. D., "Some Flutter Solutions Using Finite Element," *AIAA J.*, Vol. 8, April 1970, pp. 747–752

36. Yang, T. Y. and Sung, S. H., "Finite Element in Three-Dimensional Supersonic Unsteady Potential Flow," *AIAA J.*, Vol. 15, December 1977, pp. 1677–1683.

37. Mei, C. and Rogers, J. L., Jr., "Application of Nastran to Large Deflection Supersonic Flutter of Panels," NASA TM X-3429, October 1976, pp. 67–97.

38. Mei, C., "A Finite Element Approach for Nonlinear Panel Flutter," *AIAA J.*, Vol. 15, August 1977, pp. 1107–1110.

39. Rao, K. S. and Rao, G. V., "Large Amplitude Supersonic Flutter of Panels with Ends Elastically Restrained Against Rotation," *Computer and Structures*, Vol. 11, 1980, pp. 197–201.

40. Mei, C. and Weidman, D. J., "Nonlinear Panel Flutter—A Finite Element Approach," Computational Methods for Fluid—Structure Interaction Problems, Ed. by Belytschko, T. and Geers, T. L., AMP-Vol. 26, ASME, 1977, pp. 139–165.

41. Han, A. D. and Yang, T. Y., "Nonlinear Panel Flutter Using High Order Triangular Finite Elements," *AIAA J.*, Vol. 21, No. 10, October 1983, pp. 1453–1461.

42. Mei, C. and Wang, H. C., "Finite Element Analysis of Large Amplitude Supersonic Flutter of Panels," Proceedings International Conference on Finite Element Methods, Shanghai, China, Gordon and Breach Science Publishers, Inc., 1982, pp. 944–951.

43. Sarma, B. S. and Varadan, T. K., "Non-linear Panel Flutter by Finite Element Method," *AIAA J.*, Vol. 26, May 1988, pp. 566–574.

44. Gray, C . E., Jr., Mei, C., and Shore, C. P., "Finite Element Method for Large-Amplitude Two-Dimensional Panel Flutter at Hypersonic Speeds," *AIAA J.*, Vol. 29, February 1991, pp. 290–298.

45. Mei. C, "Nonlinear Vibration of Beams by Matrix Displacement Method," *AIAA J.*, Vol. 10, October 1972, pp. 335–357.

46. Mei, C., "Finite Element Analysis of Nonlinear Vibration of Beam Columns," *AIAA J.*, Vol. 11, April 1973, pp. 115–117.

47. Mei, C., "Finite Element Displacement Method for Large Amplitude Free Flexural Vibrations," *Computers and Structures*, Vol. 3, April 1973, pp. 163–174.

48. Dowell, E. H., *A Modern Course in Aeroelasticity*, Noorhoff, Netherlands, 1978.

49. Bisplinghoff, R. L., Ashley, H., and Halfman, R. L., *Aeroelasticity*, Addison-Wesley, Massachusetts, 1957.

50. Dowell, E. H. and Ilgamov, M., *Studies in Nonlinear Aeroelasticity*, Springer-Verlag, London, 1988.

51. Jones, R. D., *Mechanics of Composite Materials*, McGraw-Hill, New York, 1975.

52. Wood, R. D. and Schrefler, B., "Geometrically Non-Linear Analysis—A Correlation of Finite Element Notations," *International Journal for Numerical Methods in Engineering*, Vol. 12, 1978, pp. 635–642.

53. Huebner, K. H. and Thornton, E. A., *The Finite Element Method for Engineers*, Second edition, John Wiley & Sons, New York, 1982.

54. Zienkiewicz, O. C., *The Finite Element Method*, Third edition, McGraw Hill, New York, 1977.

55. Reddy, J. N., *Energy and Variational Methods in Applied Mechanics*, John Wiley & Sons, New York, 1984.

56. Bergan, P. G. and Clough, R. W., "Convergence Criteria for Iterative Processes," *AIAA J.*, Vol. 10, August 1972, pp. 1107–1108.

57. Qin, J., Gray, C. E., Jr., and Mei, C., "A Vector Unsymmetric Solver for Nonlinear Panel Flutter Analysis on High-Performance Computers," Proceedings of AIAA/ASME/ASCE/AHS/ASC 32nd Structures, Structural Dynamics and Materials Conference, Baltimore, MD, April 8–10, 1991, pp. 1971–1980.

58. Rossettos, J. N. and Tong, P., "Finite Element Analysis of Vibrations and Flutter of Cantilever Anisotropic Plates," *Journal of Applied Mechanics*, ASME Paper 74-WA/APM-15, 1974.

59. Lin, K.-J., Lu, P.-J, and Tarn, J.-Q., "Flutter Analysis of Composite Panels Using High-Precision Finite Elements," *Computer and Structures*, Vol. 33, No. 2, August 1989, pp. 561–574.

60. DOD/NASA Advanced Composite Design Guide, First Edition, Structures/Dynamics Division, Flight Dynamics Laboratories, Wright-Patterson Air Force Base, Ohio, 1983.
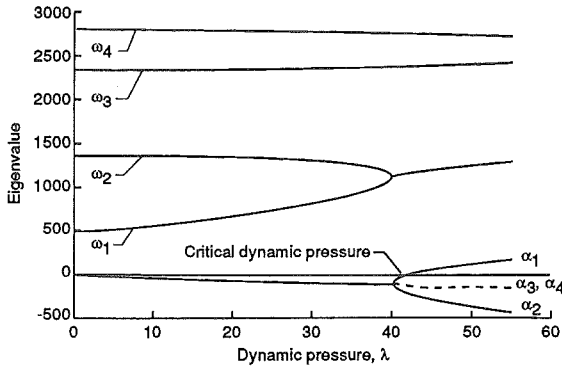
Fig. 1. Eigenvalue Variation for First Four Linear Modes of a Simply-Supported, Square Panel for Material 3. $(\mu/M = .10, Mh/a = .05)$.
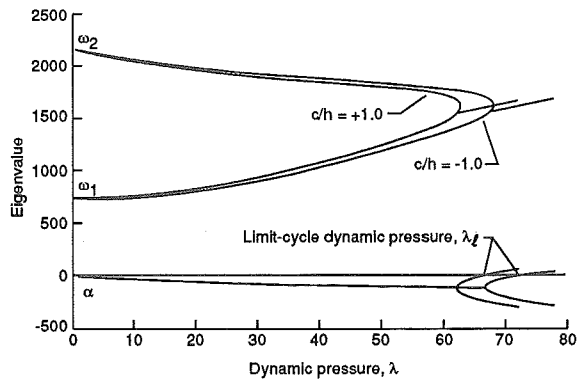
Fig. 2. Nonlinear Panel Flutter Eigenvalue Variation vs. Dynamic Pressure Using Third-Order Piston Theory Aerodynamics of a Simply-Supported, Square Panel for Material 3. $(\mu/M = .10, Mh/a = .05)$.
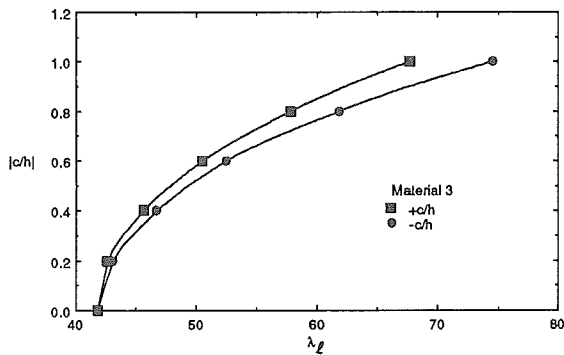
Fig. 3. Variation of Limit-Cycle Amplitude vs. Limit-Cycle Dynamic Pressure of a Simply- Supported, Square Panel for Material 3. $(\mu/M = .10, Mh/a = .05)$.
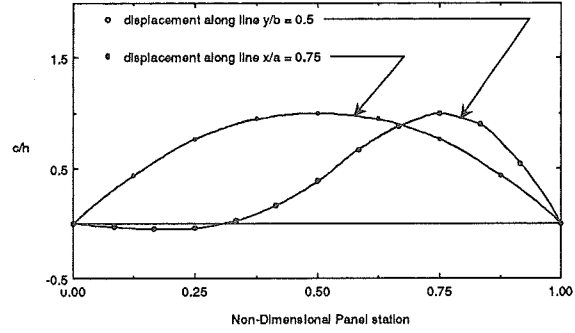
Fig. 4. Panel Limit-Cycle Deflection of a Simply-Supported, Single Layer Square Panel for Material 3. $(\mu/M = .10, Mh/a = .05, \lambda_\ell = 67.71, c/h = +1.0, 12 \times 8$ Full Panel).
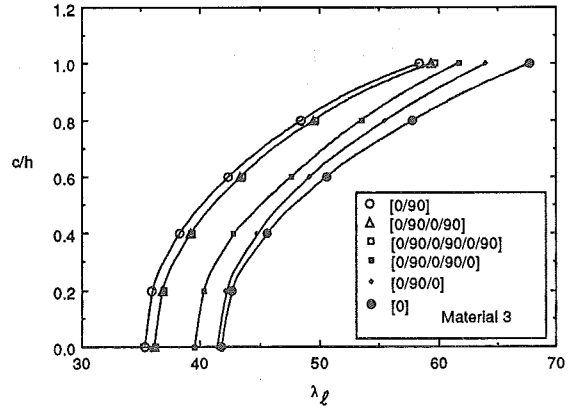
Fig. 5. Effects of Number of Plies on Limit-Cycle Amplitude and Dynamic Pressure for a Simply-Supported, Square Panel for Material 3. $(\mu/M = .10, Mh/a = .05)$.
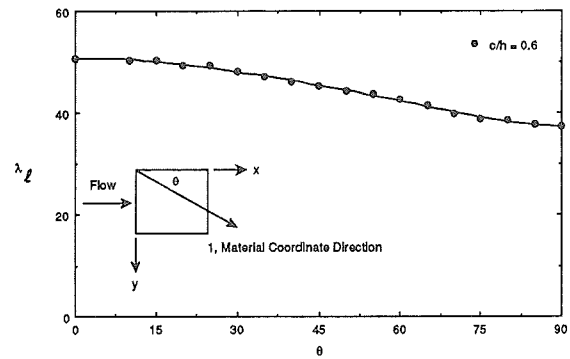
Fig. 6. Effects of Lamination Angle Variation on Limit-Cycle Dynamic Pressure for a Simply-Supported, Single Layer Square Panel for Material 3. $(\mu/M = .10, Mh/a = .05, c/h = +0.6)$.
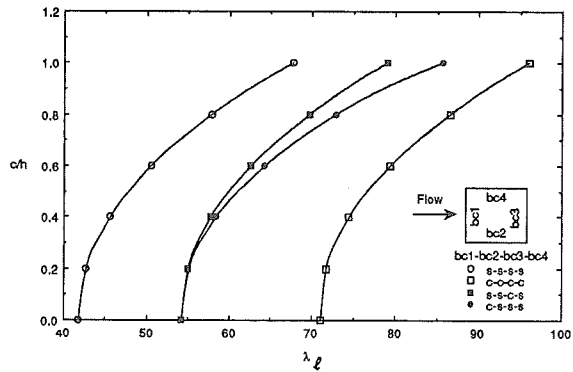
1292

Fig. 7. Limit-Cycle Amplitude at $x/a = .75$ and $y/b = .50$ vs. Dynamic Pressure for Various Support Conditions for a Single Layer Square Panel of Material 3. ($\mu/M = .10, Mh/a = .05$).
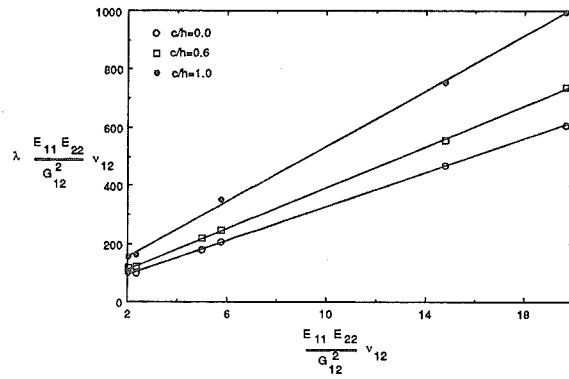

Fig. 9. Limit-Cycle Parameter vs. Orthotropic Material Parameter for Limit-Cycle Amplitudes and a Simply-Supported, Single Layer Square Panel of Material 3. ($\mu/M = .10, Mh/a = .05$).
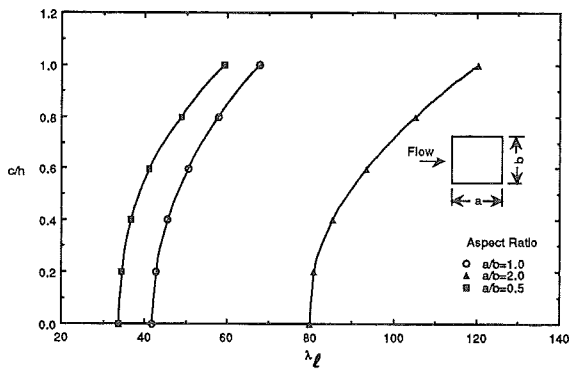

Fig. 8. Limit-Cycle Amplitude at $x/a = .75$ and $y/b = .50$ vs. Dynamic Pressure for a Simply-Supported, Single Layer Panel for Several Aspect Ratios for Material 3. ($\mu/M = .10, Mh/a = .05$).

Table 1. Panel Flutter Theories

Type	Structural Theory	Aerodynamic Theory	Range of Mach Numbers	Flutter Results
1	Linear	Linear Piston	$\sqrt{2} < M < 5$	Boundary
2	Linear	Linearized Potential Flow	$1 < M < 5$	Boundary
3	Nonlinear	Linear Piston	$\sqrt{2} < M < 5$	Limit-cycle
4	Nonlinear	Linearized Potential Flow	$1 < M < 5$	Limit-cycle
5	Nonlinear	Nonlinear Piston	$M > 5$	Limit-cycle

Table 2. Material Properties

Material Number	Material	E_{11}, Msi	E_{22}, Msi	G_{12}, Msi	ν_{12}	Weight Density, lb/in^3
1	Grs/Ep T300/5208	21.30	1.58	0.93	.38	.058
2	B/Ep Avco 5505/4	30.00	2.70	0.93	.21	.0725
3	B/Al B5.6/Al 6061-F	31.00	20.00	8.40	.27	.095
4	Steel Isotropic	30.00	30.00	11.54	.30	.283
5	Aluminum Isotropic	10.00	10.00	3.84	.30	.100

Table 3. Nonlinear Panel Flutter with Linear Aerodynamics, λ_ℓ, for 3-D Isotropic Square Panel ($E = 10$ Msi, $\nu = .3$, $\rho = .00026$ lbs-sec^2/in^4, $a = b = 12$ in, $h = 0.04$ in)

	Simply Supported		Clamped Supported	
c/h	Dowell [18]/ Eslami [32] †	Present FEM (8×4 Half Plate)	Kuo [21]/ Eslami [32] †	Present FEM (8×4 Half Plate)
0.0	540.5	535.75	881.0	887.59
0.4	578.4	583.38	940.5	940.12
0.8	724.8	731.53	1081.1	1100.67

†Values read for charts, $\lambda = \frac{2qa^3}{MD}$

Table 4. Linear Panel Flutter, λ_{cr}, for 3-D Anisotropic Cantilever Square Panel ($E_{11}/E_{22} = 2.$, $G_{12}/E_{22} = 0.364$, $\nu_{12} = .24$, $\rho = .00026$ lbs-sec^2/in^4, $a = b = 12$ in, $h = 0.04$ in)

Solution Method	Lamination Angle		
	$\theta = 15°$	$\theta = 45°$	$\theta = 90°$
Lin et al. [59]	2.470	3.920	3.455
Rossettos and Tong [58]	2.385	4.055	3.505
Present FEM (5×5 Full Plate)	2.386	4.060	3.507

$\lambda_{cr} = \frac{2qa^3}{MD_c}$, where $D_c = E_{22}h^3$

Table 5. Effects on Limit-Cycle Dynamic Pressure by Neglecting Higher-Order Terms in Aerodynamic Piston Theory[a]

Case	π_{1t}	π_{1x}	π_{2t}	π_{2x}	π_{3t}	π_{3x}	Isotropic	Single Layer	Three Layer [0/90/0]
1	1	1	0	0	0	0	82.52	70.34	66.38
2	1	1	1	0	0	0	79.93	70.12	66.24
3	1	1	0	1	0	0	77.00	67.61	63.90
4	1	1	1	1	0	0	77.42	67.82	64.15
5	1	1	1	1	1	0	77.42	67.82	64.15
6	1	1	1	1	0	1	77.19	67.69	64.03
7	1	1	1	1	1	1	77.30	67.71	64.05

[a] Simply Supported, $\mu/M = 0.1$, $Mh/a = 0.05$, $c/h = 1.0$

Table 6. Effects on Limit-Cycle Dynamic Pressure by Neglecting Higher-Order Terms in Aerodynamic Piston Theory[a]

Case	π_{1t}	π_{1x}	π_{2t}	π_{2x}	π_{3t}	π_{3x}	Isotropic	Single Layer	Three Layer [0/90/0]
1	1	1	0	0	0	0	73.56	65.13	61.67
2	1	1	1	0	0	0	73.55	65.13	61.70
3	1	1	0	1	0	0	71.11	62.88	59.61
4	1	1	1	1	0	0	71.10	62.88	59.65
5	1	1	1	1	1	0	71.10	62.88	59.65
6	1	1	1	1	0	1	70.98	62.77	59.55
7	1	1	1	1	1	1	70.98	62.78	59.54

[a] Simply Supported, $\mu/M = 0.01$, $Mh/a = 0.05$, $c/h = 1.0$